Development of a line module type of SiC deformable mirror

Pilseong Kang, Youngsoo Kim, Eui-Seung Son, Kihun Lee, Jaehyun Lee & Hyug-Gyo Rhee

Published online: 03 Mar 2025.

Submit your article to this journal ☐

Article views: 3

View related articles ☐

View Crossmark data ☐

Taylor & Francis
Taylor & Francis Group

🔓 OPEN ACCESS | Check for updates

Development of a line module type of SiC deformable mirror

Pilseong Kang[a] 🆔, Youngsoo Kim[b], Eui-Seung Son[c], Kihun Lee[c], Jaehyun Lee[a] 🆔, and Hyug-Gyo Rhee[a,d] 🆔

aDivision of Physical Metrology, Korea Research Institute of Standards and Science, Daejeon, Korea; bHanwha Systems, Seongnam-si, Korea; cDefense Rapid Acquisition Technology Research Institute, Seoul, Korea; dDepartment of Precision Measurement, University of Science and Technology, Daejeon, Korea

ABSTRACT

In this work, the complete development of a line module type silicon carbide (SiC) deformable mirror (DM) for adaptive optics (AO) is described. To eliminate the risk of fracture and misalignment during the simultaneous assembly of all actuators and the base plate of a DM, the line module concept is introduced. This line module is a pre-assembled set consisting of a line-shaped base plate to which actuators and flexures are glued in a row. This concept helps reduce the risk of actuator breakage during the assembly process while also providing flexibility by enabling the easy exchange of the line module if defective actuators are found. Flexible stand mounts are used to minimize mirror surface distortion caused by mounting. Distortions of the mirror faceplate in the complete assembly of the DM, caused by assembly tolerances, gravity, and temperature variations, are assessed through simulations. Considering the flattening of the mirror faceplate to its initial state, the distortions are found to be sufficiently low. Finally, the mirror surface stroke is checked with an interferometer, and the dynamic responses and coupling ratios are measured using a laser displacement sensor. The results show that the line module type SiC DM fulfils the design goals.

1. Introduction

Adaptive optics (AO) is an optical system capable of offsetting wavefront errors. The core components of an AO system are the wavefront error sensor, the deformable mirror, and the controller. Briefly, after the distorted wavefront of light enters the AO system, a wavefront sensor detects the wavefront error, and the wavefront error is then compensated using a deformable mirror by controlling the surface shape of the mirror. Over the past several decades, AO has achieved great success in a variety of research fields. These systems are applied in various fields, such as astronomy, microscopy, and ophthalmology, among others.[1–9] In most of these applications, the AO system is used to obtain clearer images of stars, cells, and the retina, among others, by removing the effects of turbulence. AO systems have also been applied to various high-power laser (HPL) fields, including those in science, industry, and laser weapons, among others.[10–22] To reduce thermal

CONTACT Jaehyun Lee ✉ j.lee@kriss.re.kr 🖃 Division of Physical Metrology, Korea Research Institute of Standards and Science, Daejeon, Korea; Hyug-Gyo Rhee ✉ hrhee@kriss.re.kr 🖃 Division of Physical Metrology, Korea Research Institute of Standards and Science, Daejeon, Korea, Department of Precision Measurement, University of Science and Technology, Daejeon, Korea.

deformation caused by high-power lasers, various cooling systems have been developed, including water cooling, air cooling, copper implantation, and others. Additionally, various techniques have been developed to enhance laser beam quality and mitigate the effects of strong atmospheric turbulence. There is also research on defining criteria and factors for evaluating the improvements in beam quality achieved by AO. In HPL applications, AO systems are effective in concentrating energy because the wavefront errors caused by atmospheric turbulence cannot be neglected when the objective path length is long and shorter-wavelength lasers are used.[23]

The deformable mirror (DM) is an essential component, and it was initially adopted in AO research by H. W. Babcock in 1953.[24] The DM can cancel the wavefront error out from the distorted light through physical deformation of the reflecting mirror. In general, a DM consists of a mirror faceplate, actuators, and a base plate [16]. The material of a mirror faceplate is determined by the application of the DM. According to the range of the wavefront error to be compensated for by the AO system, the diameter and thickness of the mirror faceplate are determined. A piezoelectric (lead-zirconium-titanium oxide, PZT) actuator can stretch in its longitudinal direction with a supply of electric power. When the actuators push up and pull down the mirror faceplate, the mirror surface shape changes. With more actuators, more complex shape changes of the mirror surface become possible. To realize this, an array of actuators on a mother plate or numerous individual actuators can be applied to a DM. The base plate is used to hold the actuators together while also providing an interface to connect to a stand mount or a tip-tilt stage. To reduce thermal deformation, a material with a low coefficient of thermal expansion is used for the base plate. All of the components of the DM are assembled using adhesive such that they are firmly held in place, and the mirror surface does not deform unexpectedly when the system is operating. The required mirror surface stroke and the spacings of the actuators are determined according to the wavefront error compensation condition, as are the diameter and thickness of the mirror faceplate and the dynamic response range of the mirror surface. Given that all components of the DM are glued during the assembly process, an appropriate adhesive suitable for the specified user condition should be selected.

The entire assembly process of a DM should be handled with great care, as both the mirror faceplate and actuators are brittle. The mirror faceplate, in particular, must be carefully managed to prevent degradation of its surface quality. Additionally, all components are glued in place to minimize deformation variation of the mirror faceplate during use, making precise alignment of components before gluing crucial. Since numerous actuators must be glued to both the base plate and the mirror faceplate within a limited adhesive handling time, there is a risk of actuator breakage and misalignment. In most DM manufacturing, a single-piece base plate is used, which makes it challenging to assemble numerous actuators with precise alignment without causing part breakage, especially when using actuators that have connecting wires.

To eliminate the potential risk factors mentioned above, we have introduced a new line module concept for building a DM in this research. Instead of gluing numerous actuators onto a base plate at once, line modules are stacked horizontally into an outer base plate and then covered with a cover plate. Each line module is pre-assembled by gluing a series of actuators and flexures onto a line-shaped inner base plate. Adopting this line module concept minimizes the risk of actuator breakage

during assembly. Additionally, it offers flexibility by enabling the easy exchange of a line module if defective actuators are found. Since the inner part of the base plate is divided into several line base plates, the tolerance check for all the actuators is performed in two steps: first for each line module, and then across the line modules. Through these tolerance checks, the overall alignment of all actuators is verified to minimize deformation of the mirror faceplate after gluing. Since the horizontally stacked line modules have directionality, the deformation of the mirror surface also exhibits a directional pattern. However, the deformation is small enough to be corrected with short actuator strokes, and any temperature-induced deformation can be restored within the elastic range.

In this paper, the full development process of a line module type silicon carbide (SiC) DM for AO is presented. Considering the operating conditions of the DM in Korean atmospheric conditions, specifications such as the diameter and thickness of the mirror faceplate, the sizes and spacings of the actuators, the stroke of a single actuator, and the mirror surface stroke are determined. During the structural design phase, the shape and sizes of the flexure are optimized to meet the required mirror surface stroke and the allowable levels of adhesive stress, based on the results of previous research by the authors.[20] As noted above, all of the components of the DM are assembled using an adhesive. Thus, if all actuators are glued to the base plate at once within a short time, handling of the actuators becomes complicated, increasing the risk of damage to the brittle actuators. Since checking the heights of all the arrayed actuators at once takes too much time, it is hard to be done before the adhesive cures. Also, it is difficult to replace defective actuators after the adhesive is cured. Thus, in the present research, the line module concept is adopted. The base plate is divided into the outer and inner parts, and the inner part is separated line by line. Each line module includes a line base plate and several actuators arranged in a row. After all of the line modules are prepared, the line modules are glued together into the outer part of the base plate. As mentioned above, the line module concept allows easy checking of the heights of the actuators within a line module and provides the opportunity to replace a line module with a defective actuator by a spare line module during the line module assembly process. To minimize the deterioration of the mirror surface quality during the assembly process, delicate assembly methods are applied one step at a time. Finally, the fully assembled DM is fixed in the horizontal direction with two bipod stands and a bottom flexure, thus reducing mirror distortion caused by the mounting process. Tests are conducted to validate the hardware performance. The mirror surface stroke is checked with an interferometer, and the dynamic responses and the coupling ratios are measured with a laser displacement sensor.

Section 2 introduces the components of the DM. Section 3 presents the prediction of the mirror surface stroke of the designed DM using finite element analysis (FEA), along with simulations of deformations due to gravity and temperature variations. Section 4 describes the assembly process of the DM. Section 5 presents the hardware performance tests of the DM, along with the results. Finally, section 6 concludes the present research.

2. Components of the line-module-type SiC DM

2.1. Fully assembled DM

A 3D model of the SiC DM developed in the present research is shown in Figure 1. The major components of the DM are its mirror faceplate, flexures, actuators, and base plate. As shown in Figure 2, the DM is mounted horizontally with bipod stands and a bottom flexure to minimize the deformation of the mirror faceplate. Pivot cylinders are attached to both sides of the DM, and inserted into the holes of the bipod stands to reduce torsion.

All components of the DM are glued together using epoxy adhesive, as shown in Figure 3. An actuator, consisting of the top and bottom isolation caps with the middle multilayer actuator part, is inserted into the square hole of the base plate and glued in place. A flexure is glued to the top of the actuator, between the mirror faceplate and the actuator. To increase the gluing

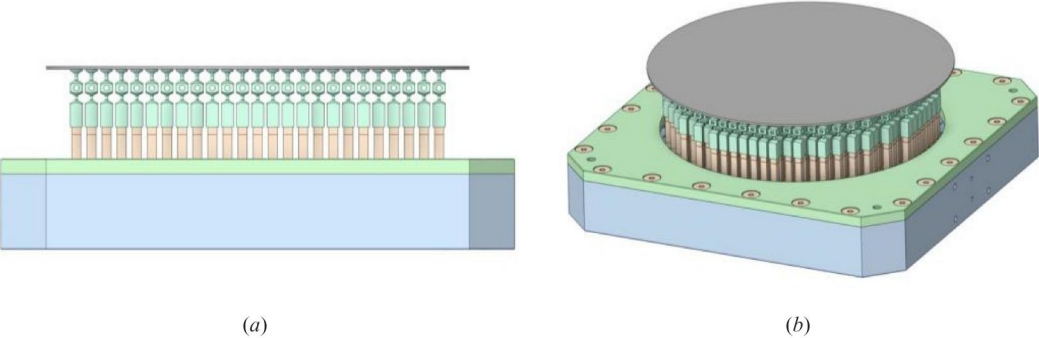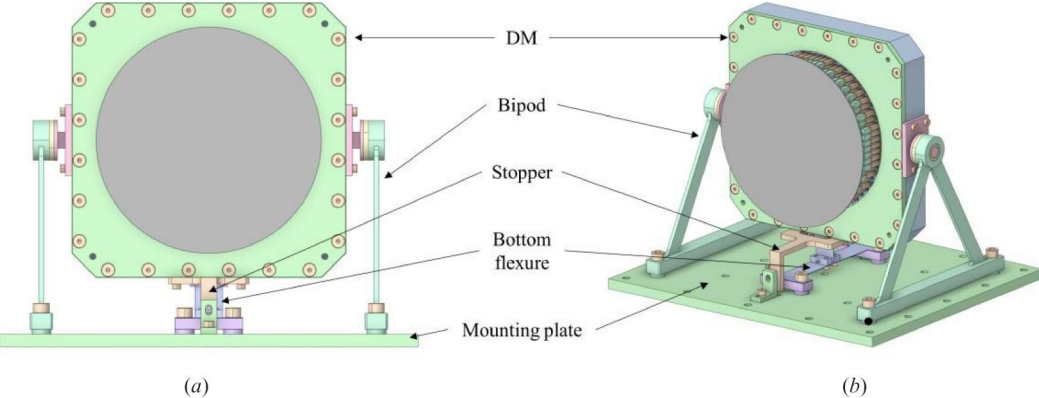**Figure 1.** Line module type SiC DM: (a) front view, (b) trimetric view.

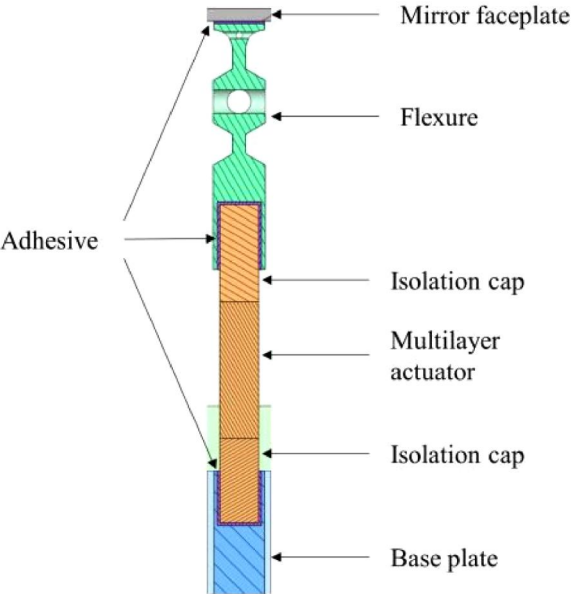**Figure 2.** Line module type SiC DM with mounting stands: (a) front view, (b) trimetric view.

Figure 3. Cross-sectional view of the DM corresponding to one actuator.

area, the bottom of the flexure is hollowed into a square shape. The top side of the flexure is then glued to the bottom of the mirror faceplate.

At the bottom, a thick base plate serves to hold the actuators. It is divided into an outer base plate, inner line base plates, and a cover. Each line module is a pre-assembled set consisting of a line base plate, actuators, and flexures. The line modules are stacked horizontally into the outer base plate and then covered with the cover plate. An array of discrete actuators, placed perpendicular to the mirror faceplate with specific spacings in the x- and y-directions, is used to generate surface strokes. By applying electric power to the actuators, the longitudinal actuator strokes cause the mirror surface shape to change. The flexure structure is placed between the mirror faceplate and the actuator. It is designed such that it efficiently concentrates the force transmitted from the actuators and transmits it to the mirror faceplate. It also contributes to reducing the adhesive stress under the operating conditions. The cylindrical necks of the flexure concentrate the actuator force at the center of the attachment area on the mirror faceplate. Additionally, the necks are easily bent, reducing the bending stress on the actuator. A large, thin SiC mirror faceplate manufactured by chemical vapor deposition (CVD) is applied to the DM considering HPL applications. SiC is increasingly being used for mirror faceplates due to its superior mechanical and thermal properties compared to conventional glass materials. It enables extremely high surface figure precision ($\lambda/20$) and very low surface roughness ($\sim$0.1 nm).[26] Thanks to its high specific stiffness (Young's modulus/density), the quilting effect on the mirror surface is minimized, and deformation due to the coolant flow in cooled DMs is reduced. The high thermal stability (thermal conductivity/(thermal expansion × specific heat)) of SiC reduces distortions caused by temperature changes. Additionally, the high thermal diffusivity (thermal conductivity/thermal expansion) of SiC allows it to transmit heat faster than glass.[17,25] This results in better temperature control and stability in high-power laser applications. While SiC is a brittle material, its bending strength is superior to that of glass materials used as mirror faceplates in DMs. During the assembly of the components of the DM, epoxy adhesive (3 M® EC2216 B/A gray) is used. This adhesive exhibits high shear and peel strength while maintaining excellent flexibility. It is also resistant to extreme shock, vibration, and flexing. Additionally, it has been tested and certified for aircraft and aerospace applications.[27] Invar36 given its extremely low coefficient of thermal expansion (CTE) is used for the base plate and flexures. The mechanical properties of the materials used to create the components are shown in Table 1.

Considering the atmospheric conditions in Korea, the target values for the stroke and dynamic response of the mirror surface due to a single actuator operation in the developed DM are 2 μm and 1 kHz, respectively. The allowable coupling ratio range is 15–70%.

2.2. A thin SiC mirror faceplate

To correct the wavefront error induced by atmospheric turbulence that arises when controlling the selected actuators, a thin SiC mirror is needed. The stiffness of SiC is very high, so larger strokes and greater forces from the actuators are needed to achieve the designated mirror surface strokes. In contrast, if the mirror faceplate is too thin, the mirror surface stroke may increase, but the influence function becomes too narrow or a quilting effect may occur. During the fabrication and polishing of the mirror faceplate, the desired surface figure quality may not be achieved if the mirror is too thin.

Table 1. Mechanical properties of key materials.

Material	Young's modulus (GPa)	Poisson's ratio	Density (kg/m^3)	CTE (10^{-6} m/m/°C)
Invar36	141	0.259	8,050	1.26
SiC	419	0.16	3,130	4.0
PZT (cap)	52.4	0.35	7,800	8.0
PZT (actuator)	62.3 (x, y) 32.0 (z)	0.34	8,000	6.0 (x, y) 3.0 (z)
EC2216 Gray	0.69	0.43	1,320	102

(a)   *(b)*   *(c)*
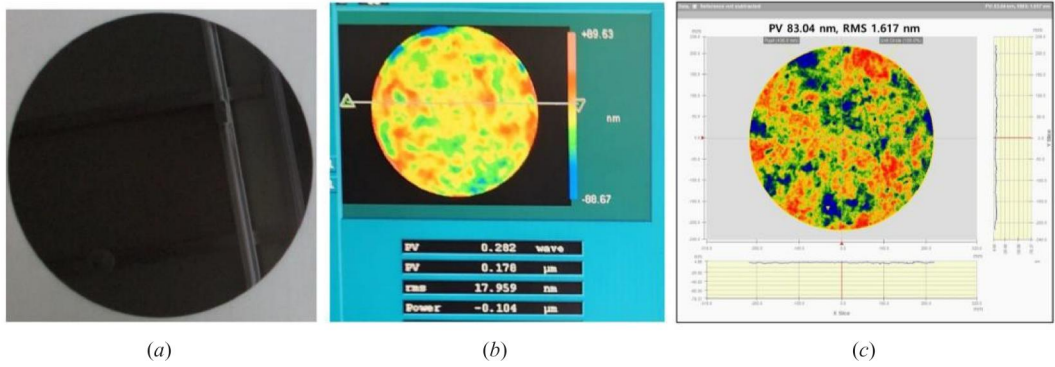
Figure 4. Fabricated SiC mirror faceplate: (a) mirror faceplate, (b) flatness measurement result (PV 178 nm, RMS 17.96 nm), and (c) roughness measurement result (PV 83.04 nm, RMS 1.62 nm).

Considering the factors mentioned above, the thickness of the SiC mirror faceplate for the DM is determined to be between 0.95 and 1.0 mm, accounting for the reduction in thickness during the polishing phase. The thin SiC mirror faceplate is precisely fabricated using the adaptive hydrostatic pressure control fabrication method developed at the Korea Research Institute of Standards and Science. In this way, the SiC mirror faceplate is successfully fabricated, and Figure 4 shows the result. Its surface flatness and roughness are measured by a Zygo® Fizeau interferometer and a white light interferometer, respectively, with the corresponding results being 17.96 nm RMS and 1.62 nm RMS, respectively, with a clear aperture diameter of 120 mm.

2.3. Actuator and flexure

To control the mirror surface stroke during high-frequency operation in AO, PZT actuators were utilized. We used commercial actuators and, after considering specifications such as stroke, blocking force, and driving frequency, selected one from the available product range. The selected PZT actuator is shown in Figure 5(a). Its nominal stroke and blocking force are 11 μm and 310 N, respectively, with a driving frequency greater than 1 kHz. The lateral dimensions are 3 mm $\times$ 3 mm, and the length, including the top and bottom insulation caps, is approximately 25 mm. To ensure a sufficient gluing area, a cup-shaped design for the bottom of the flexure was introduced, as shown in Figure 5(b). The inner surfaces of the square cup are glued to the surfaces of the top cap of the actuator.

When operating, the inner actuators are active, but the actuators at the boundary (marked in red in Figure 6) are used to support the mirror faceplate.

2.4. Design of flexures

The mirror faceplate is deformed by the push-up and pull-down motions of the actuators. Thus, the range of the mirror surface stroke is affected by the solidity of glue between the mirror faceplate and the actuators. According to the previous research of our research group,[20] the direct gluing between these components would be best for solidity, but doing so overstresses the adhesive between them and reduces the mirror surface stroke given the square shape of the top cap of the actuator. Since gluing area is a rectangular-shaped, the forces from the actuator cannot be concentrated, and the bending stiffness at the glued region becomes excessive. To resolve these problems, in the previous research, flexures are adopted between the mirror faceplate and the actuators. By changing the head shape of the flexure, the gluing area and shape are modified, reducing the stress at the corners of the square-shaped gluing. The lengths of the top and bottom necks of the flexure, as well as the hole diameter of the middle box between the necks, can be
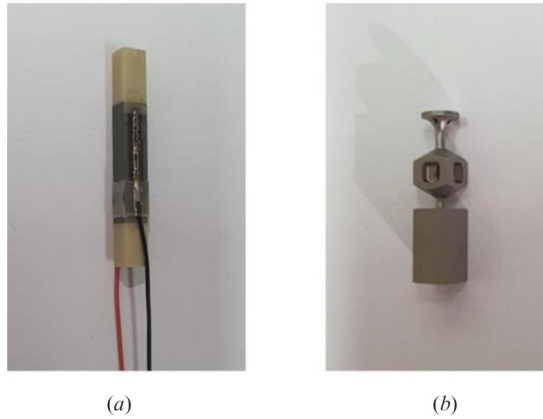
(a)   (b)

Figure 5. Actuator and flexure: (a) PZT actuator with PZT insulation caps, (b) Invar36 flexure.

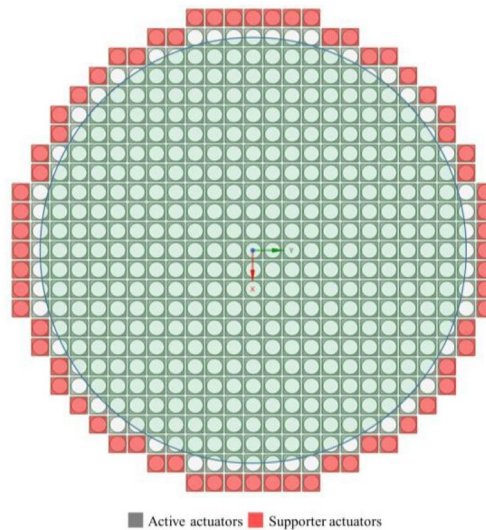■ Active actuators ■ Supporter actuators

Figure 6. Layout of actuators.

adjusted to control the longitudinal stiffness of the flexure. The cylindrical neck concentrates the force generated by the actuator, which has a square cross-section. Additionally, the necks, being more flexible in bending, reduce the bending stress on the actuator caused by the movements of neighboring actuators. The gluing area at the bottom of the flexure can be adjusted by considering the adhesive stress caused by the full stroke of the actuator. As mentioned above, a cup shape is applied in this research to enlarge the gluing surface.

Structural optimization of the flexure for the DM was also conducted in the previous research. In that study, the target DM was an engineering model with 5×5 actuators intended to reduce the complexity of the full-channel DM. First, topology optimization to maximize the mirror surface stroke was performed using GTAM in ANSYS®. Based on the optimal topology result, the initial design of the flexure was devised. The major dimensions of the initial flexure design were optimized using response surface optimization with ANSYS® DesignXplorer. The outcome showed that the optimal shape of the flexure met the required mirror surface stroke and adhesive stresses requirements.

The optimized flexure from our previous study was then adjusted to ensure proper performance for the full-channel DM in the present research. The overall shape remains unchanged, but

the neck length and bonding areas of the top side, as well as the bottom cup-shaped surface, were adjusted based on the mirror surface stroke and adhesive stresses through simulations for the full-channel DM. The lateral dimensions of the flexure are 4 mm × 4 mm, with a height of approximately 20 mm, as shown in Figure 5(b).

2.5. Base plate

A base plate consisting of Invar36 is introduced at the bottom of the DM. The thickness of the base plate is designed to be as light as possible while preventing deformation due to the actuator operation. In addition, since the actuators, flexures, and mirror faceplate are stacked and bonded to the base plate, the flatness and parallelism of the top and bottom sides during manufacturing are maintained within 20 μm. As shown in Figure 7, square holes are drilled into the top of the base plate to increase the gluing area with actuators. The base plate is divided into outer and inner parts, and the inner part is separated line by line. Each line of the base plate has square holes in which to plant an actuator along with wire grooves on both sides. To ensure alignment across the line base plates, they are manufactured so that the tolerance of the dimensions from the attaching sides on the reference sides of the outer base plate to the bottom sides of the square holes is within 20 μm. The line base plates are attached to each other by gluing. Therefore, the gap between the line base plates is determined by considering the adhesive thickness. During thermal deformation due to the temperature changes, the deformations of the line base plates are not irregular when the adhesive thicknesses are consistent. Therefore, they are manufactured in a way that the tolerance of the widths of the line base plates is also no more than 50 μm. To fix the lined base plates onto the outer base plate, two end points of each lined base plate are fixed with bolts. After gluing the outer and the line base plates, a cover plate is placed over them.

3. Simulation results of the SiC DM

3.1. Finite element model and boundary conditions

We checked the full strokes of all actuators, approximately seven hundred including spares, and the results show that the maximum, minimum, and average strokes of them are 14.1 μm, 7.8 μm, and 11.1 μm, respectively. Accounting for the safety margin and the expected stroke for the mirror

(a)   (b)
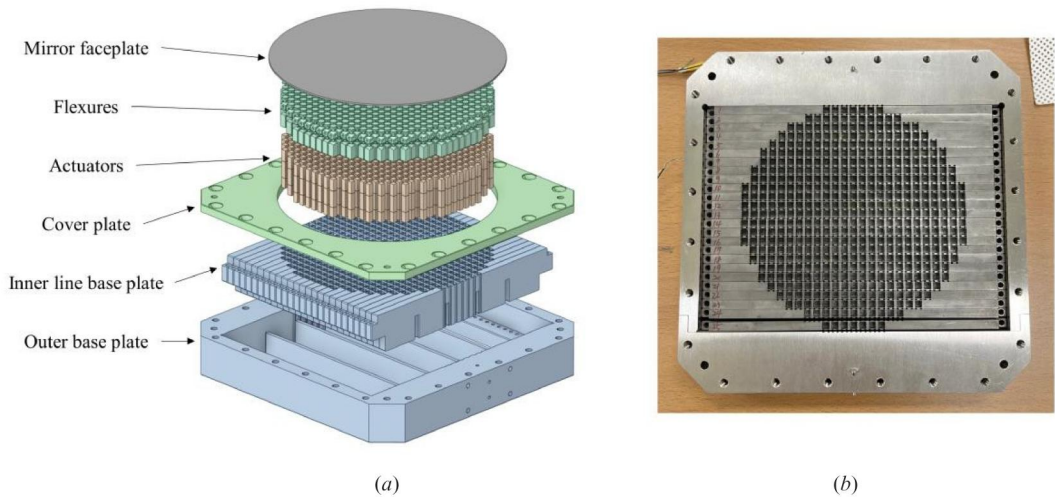
Figure 7. Base plate: (a) exploded view of the line-module-type SiC DM, (b) manufactured outer and inner line base plates.
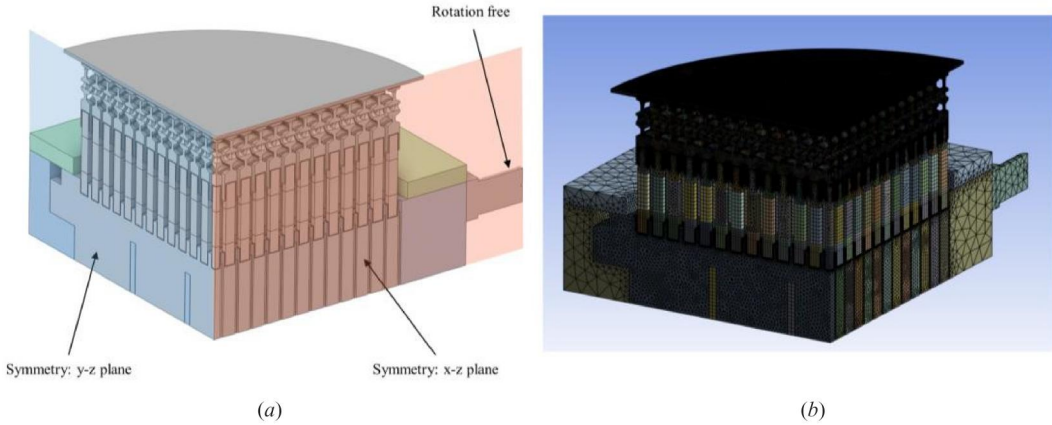
Figure 8. Analysis model of the SiC DM: (a) quarter model and boundary conditions, (b) FE model.

faceplate flattening, the reference stroke of an actuator is determined as 7.9 μm. The mirror surface stroke of the SiC DM by a single actuator stroke of 7.9 μm is designed to be 2 μm or more. To verify the mirror surface stroke, FEA is performed using ANSYS® mechanical. Additionally, deformation of the mirror surface due to gravity is considered, as it occurs naturally when the DM is installed horizontally in an AO system. Lastly, a thermal analysis is conducted, and the wavefront error of the mirror faceplate is analyzed. The boundary conditions are shown in Figure 8(a).

Considering the symmetry of the DM structure, it can be modeled as a quarter model with plane symmetry boundary conditions applied to the planes normal to the x- and y-axes to reduce computational effort. As shown in Figure 2, the DM is mounted horizontally with mounting stands. Each bipod stand is in contact with a pivot cylinder attached to the side of the outer base plate of the DM to reduce torsion at the mounting point. Therefore, rotation-free boundary conditions are applied to the outer surfaces of the pivot cylinder at the sides of the outer base plate. Figure 8(b) shows the FE model of the DM. The thin parts, such as the mirror faceplate and adhesives, are meshed with at least two layers in the thickness direction. The flexures are meshed with smaller elements than the other parts, due to their structural complexity and small dimensions. The mesh quality and solution convergence are checked by the program. The mesh sizes of all parts of the DM are determined by considering solution convergence, mesh quality, and computational efficiency. As a result, the full model of the DM is meshed with a total of 17,873,454 nodes and 11,864,435 elements.

3.2. Mirror surface stroke by a single actuator stroke

Figure 9 shows the result when a 7.9 μm stroke is applied to the center actuator. In both the push-up (Figure 9(a)) and pull-down (Figure 9(b)) cases, the mirror surface stroke (PV) is 2.11 μm. The levels of adhesive stress should not exceed the corresponding allowable levels. In earlier work by the authors,[20] the failure stress points for the adhesive between SiC and Invar36 and between Invar36 and PZT were derived from experiments, and the allowable stress levels were determined, allowing the application of a safety factor of 1.5. Simulation results for the adhesive stress are listed in Table 2. As indicated, all stress levels are below the allowable levels.

3.3. Surface error of mirror due to gravity and temperature variations

As mentioned above, the DM is installed horizontally in an AO system, meaning it is subject to the influence of gravity due to its position. The mirror surface was fabricated and polished to be flat for successful wavefront error compensation in the AO system, but the mirror surface
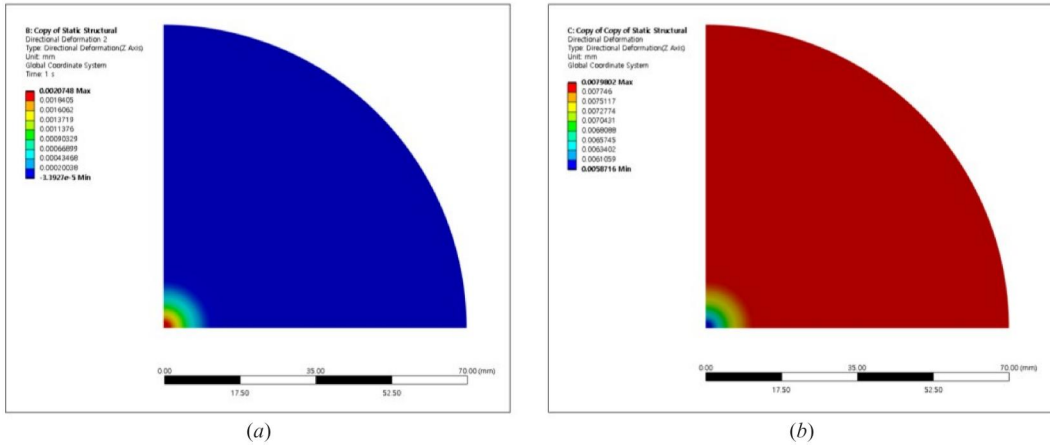
Figure 9. Analysis results: (a) 7.9 μm push-up case, (b) 7.9 μm pull-down case.

Table 2. Adhesive stress upon the operation of a single actuator.

Force condition	Adhesive position	Mirror–flexure	Flexure–actuator	Actuator–base
Allowable stresses	Normal/shear	4.13/4.06	2.60/2.47	2.60/2.47
Push-up case	Normal/shear	1.03/1.96	0.66/0.55	0.28/0.68
Pull-down case	Normal/shear	4.11/1.96	2.24/0.55	1.65/0.67

The description of the values: The unit of each value is MPa.

deforms under gravity. Because the mirror faceplate is relatively light, it is slightly deflected. As shown in Figure 10(a), the tip/tilt-removed PV and RMS values of the surface error are 15.22 nm and 2.38 nm, respectively.

The AO system, including the DM, is mostly equipped in a room where temperature and humidity are carefully controlled. However, the DM should not be allowed to deform excessively under unexpected temperature variations. To predict the amount of surface error due to temperature changes, the deformation is analyzed for a + 5 °C temperature variation. The resulting shape error for the mirror surface is shown in Figure 10(b). Due to the directional nature of the line modules, the mirror deformation occurs symmetrically about the y-axis. However, the PV and RMS values, with the tip/tilt removed, are only 108.44 nm and 16.32 nm, respectively. As stated in section 3.1, the total stroke for mirror flattening and the safety margin is 3.2 μm. This stroke allows the mirror surface deformation to be corrected by up to approximately 850 nm RMS. Therefore, it is sufficient to compensate for the mirror surface deformation due to gravity and temperature changes, and the resulting shape error can be considered negligible. In addition, the deformations occur within the elastic range, and the mirror shape is restored once the heat is removed.

In both the gravity and thermal analyses, it was found that the stress levels of all components of the DM, including the adhesives, did not exceed the corresponding allowable limits.

3.4. Mirror surface deformation according to the assembly tolerance of bipod stands

To reduce the mirror deformation during the mounting step, two bipod stands and a bottom flexure are applied, as shown in Figure 11. Additionally, a stopper is applied to the bottom of the DM to prevent damage in case the DM is unintentionally rotated. The bipod stands are flexible enough to reduce the mirror surface distortion, but mirror distortion may occur if the bipod stands are fixed in an incorrect posture or a slip of the fixed point of the bipod when fastening a bolt. Therefore, the mirror deformation resulting from deviations in the fixed positions is
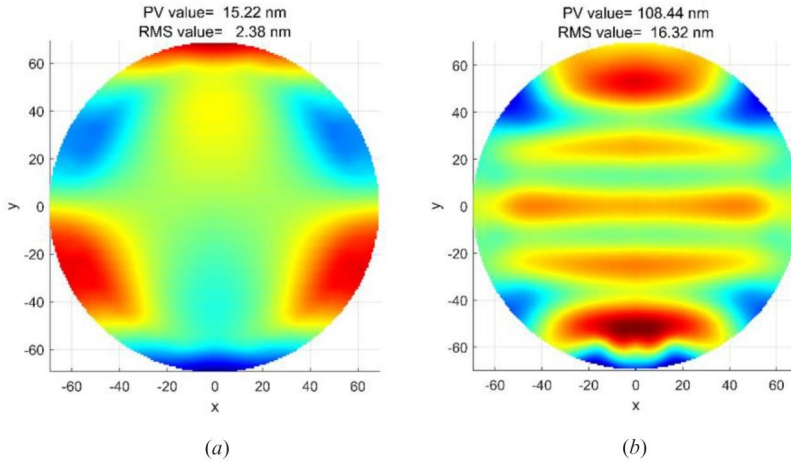
Figure 10. Analysis results: (a) surface error of mirror under gravity of the DM in the y direction, (b) surface error of the mirror in during a + 5 °C temperature change.
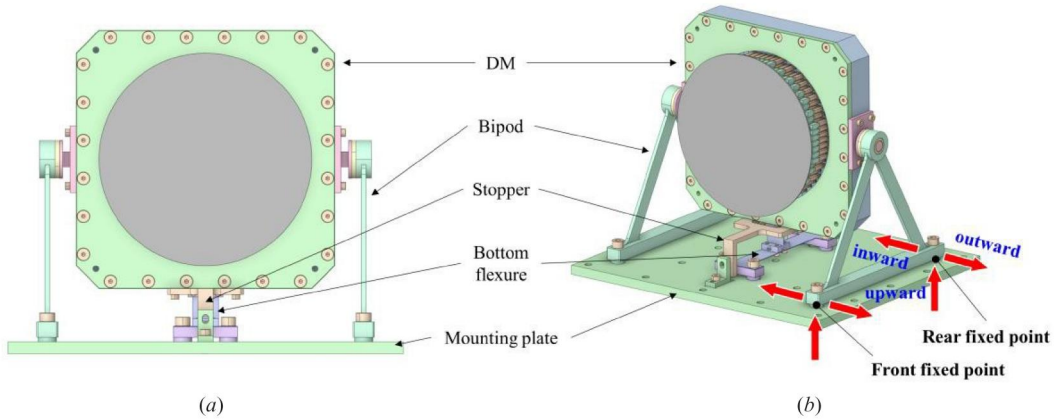

Figure 11. DM fixed with the bipod stands and bottom flexure, where the arrows represent the deviation direction of the fixed position.

simulated and analyzed. The tolerance of the hole positions in the mounting plate is controlled within 100 μm during fabrication. Position errors due to the misalignment or slippage from bolt fastening can range from tens to hundreds of microns. We analyzed the surface deformations based on a 0.1 mm variation of each fixed point in each direction. The mirror surface error can be estimated linearly for larger variations.

Figure 12 shows the deformations of the mirror surface due to the six deviations of the fixed positions. The PV and RMS values are under 1 nm, indicating that the bipod stands effectively prevent distortion of the mirror surface.

4. DM assembly process

The assembly of the DM is a very delicate process, with much labor required for every step. Most importantly, the flatness of the high-precision fabricated mirror surface should be maintained until the end of the assembly process. Handling of the ceramic-based actuator must be carefully done due to its brittleness and the presence of the electrode. Also, the lateral spacings of the
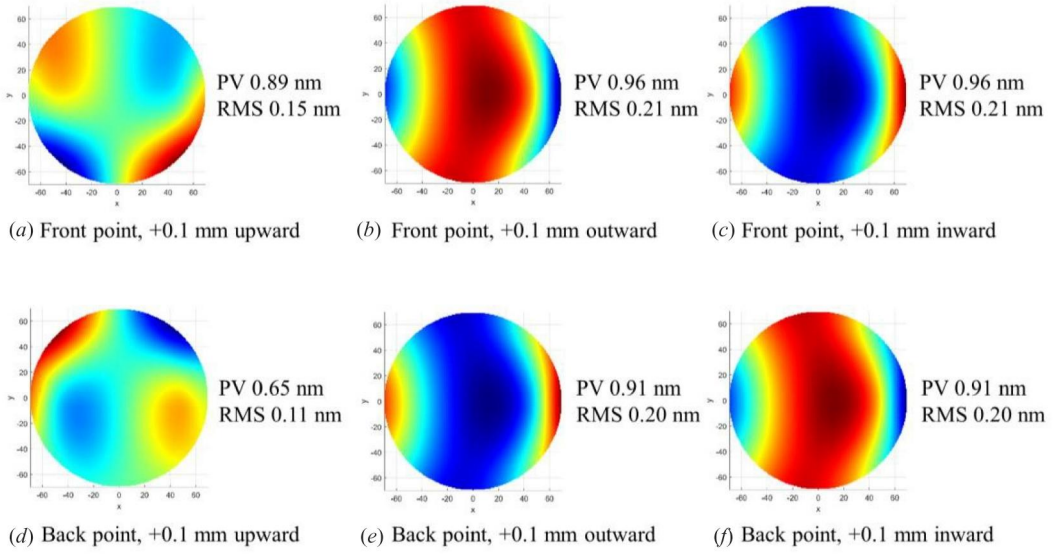
Figure 12. Analysis results: (a) + 0.1 mm upward deviation at the front fixed point, (b) + 0.1 mm outward deviation at the front fixed point, (c) + 0.1 mm inward deviation at the front fixed point, (d) + 0.1 mm upward deviation at the back fixed point, (e) + 0.1 mm outward deviation at the back fixed point, and (f) + 0.1 mm inward deviation at the back fixed point.
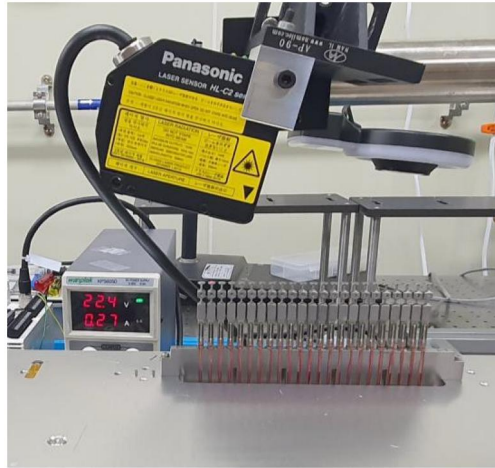

Figure 13. Checking the heights of the flexures in a line module.

actuators are kept regularly as they are designed, and the thickness of every adhesive should be within the optimal thickness range of 150–250 μm obtained through in-house experiments.

For this challenging work, we assemble all parts in a stepwise manner with precision-fabricated flexible spacers and fixtures. First, each line base plate and the corresponding number of actuators are glued adhesive. Before and after the adhesive has cured, the heights of the actuators in a row are checked with a coordinate-measuring machine (CMM). Considering the optimal adhesive thickness, the flatness of the top of the actuators is measured as to whether it is within ± 50 μm. Subsequently, the flexures are glued to the top of the actuators already installed in the line base plate while maintaining the flatness of the top of the flexures within ± 50 μm. The final line module consists of a line base plate and actuators and flexures. The gluing quality of the assembled line modules is checked, and the heights of the flexures in a line module are measured, as shown in Figure 13.
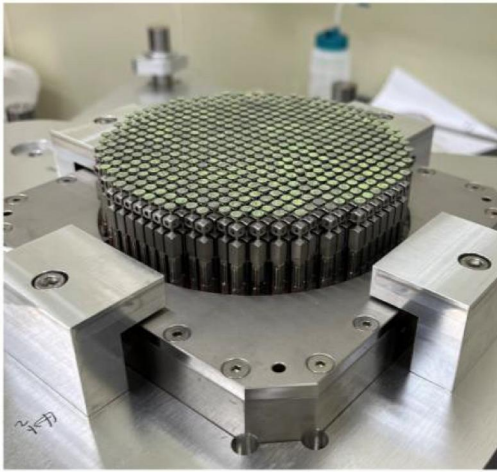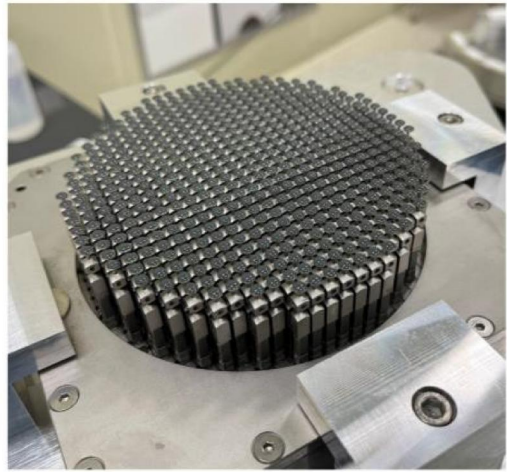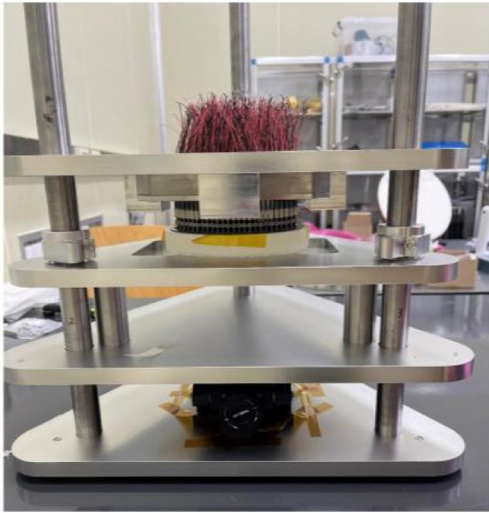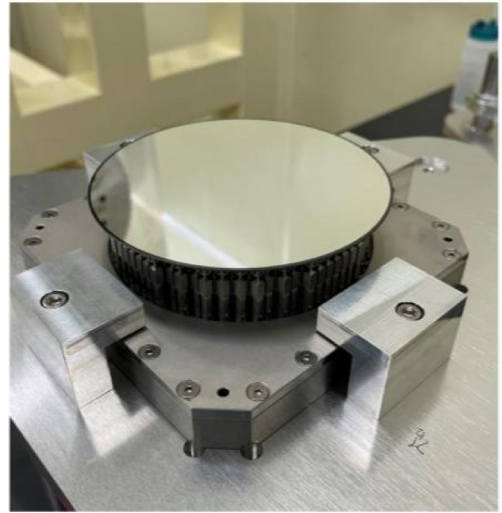
Figure 14. Bottom assembly: (a) assembly of base plate, actuators, and flexures; and (b) adhesive applied to the top of the flexures.

Figure 15. Assembly process of the bottom module and mirror faceplate: (a) flipped bottom module and mirror faceplate, (b) fully assembled SiC DM.

The prepared line modules are stacked in a parallel manner inside the outer base plate. The end points of each line module are bolted to the outer base plate, and adhesive is applied between the line modules. Finally, the cover plate is bolted on top of the outer base plate. Primer is applied to the top surfaces of the flexures, as shown in Figure 14(a), and adhesive is applied to the top of the flexures, as shown in Figure 14(b).

Figure 15(a) shows the gluing process of the bottom assembly (assembly of the base plate, the actuators, and the flexures) and the mirror faceplate. The flipped bottom assembly is attached to the mirror faceplate positioned on a precision-fabricated glass plate. The main reasons for introducing this assembly process are to prevent the application of force to the mirror faceplate and to maintain the ideal adhesive thickness between the mirror faceplate and the flexures. After

curing, all fixtures are removed and all assembly processes are completed. Figure 15(b) presents the fully assembled SiC DM.

5. Performance test of the DM

5.1. Test of the mirror surface stroke

One of the major items affecting the DM performance is the mirror surface stroke. In this section, the mirror surface stroke of the developed DM is tested. As shown in Figure 16, the mirror surface stroke is measured by a Fizeau interferometer by applying voltage at each actuator. Electric power is applied to each active actuator to generate a 7.9 μm actuator stroke.

Influence function maps of one quadrant, including the center lines in the horizontal and the vertical directions, are shown in Figure 17. Each influence function map means the level of contribution on the wavefront correction of each actuator. Each small circular figure in Figure 17 is the surface map when the actuator at the figure's position is activated. The portions of the influence map marked in red apart from the activated actuator position are the deformations due to the result of mirror surface coating and the residual currents of the actuators. Considering these aspects, it is confirmed that the mirror surface at each active actuator is properly deformed. Figure 18 represents the mirror surface strokes in all actuator positions. The average stoke is 3.0 μm, and the maximum and minimum values are 3.70 μm and 2.04 μm, respectively. As indicated, all strokes exceed 2.0 μm, and the DM satisfies the design target: mirror surface stroke by a 7.9 μm single actuator stoke $\geq$ 2.0 μm.

5.2. Test of the dynamic response of the actuators

The mirror surface stroke of the DM should show a high dynamic response for reliable wavefront error correction in an AO system. Here, test equipment is used to measure the dynamic response of the DM, as shown in Figure 19. Electric power is supplied to the DM through a function generator and relay switches. The function generator supplies a 1 kHz frequency input of power, and the relay switches automatically select an actuator channel to be powered by a sequential program. To measure the dynamic mirror stroke, a high-resolution laser displacement sensor is applied. The laser sensor is attached to a two-axis motorized stage, and its position is controlled by the program. The dynamic mirror stroke is measured by the sensor, and the stroke changes during the measurement time are displayed on a laptop monitor.
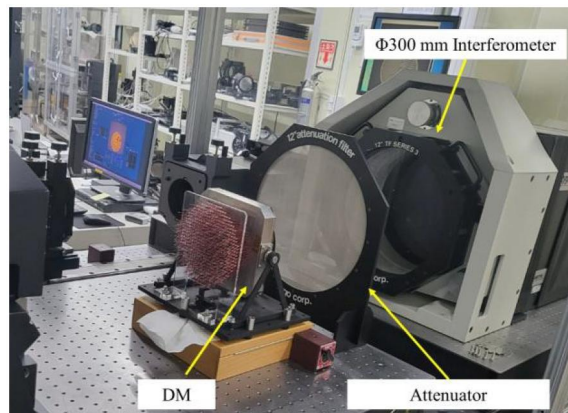

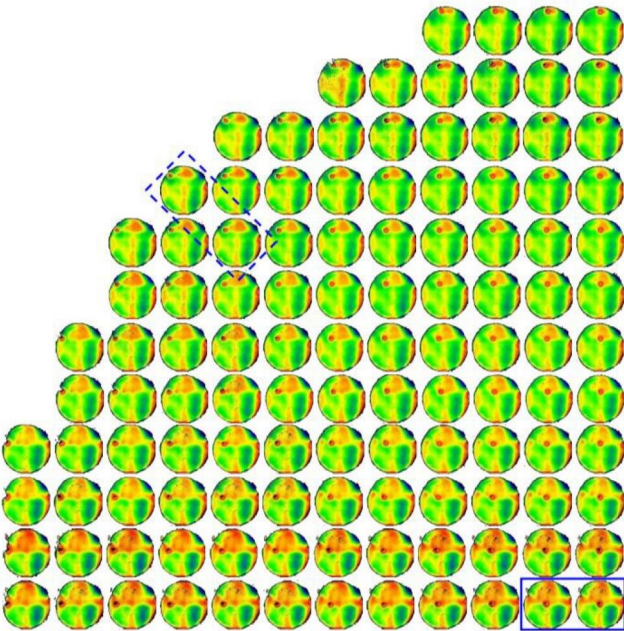**Figure 16.** Measurement of the mirror surface stroke using a Fizeau interferometer.

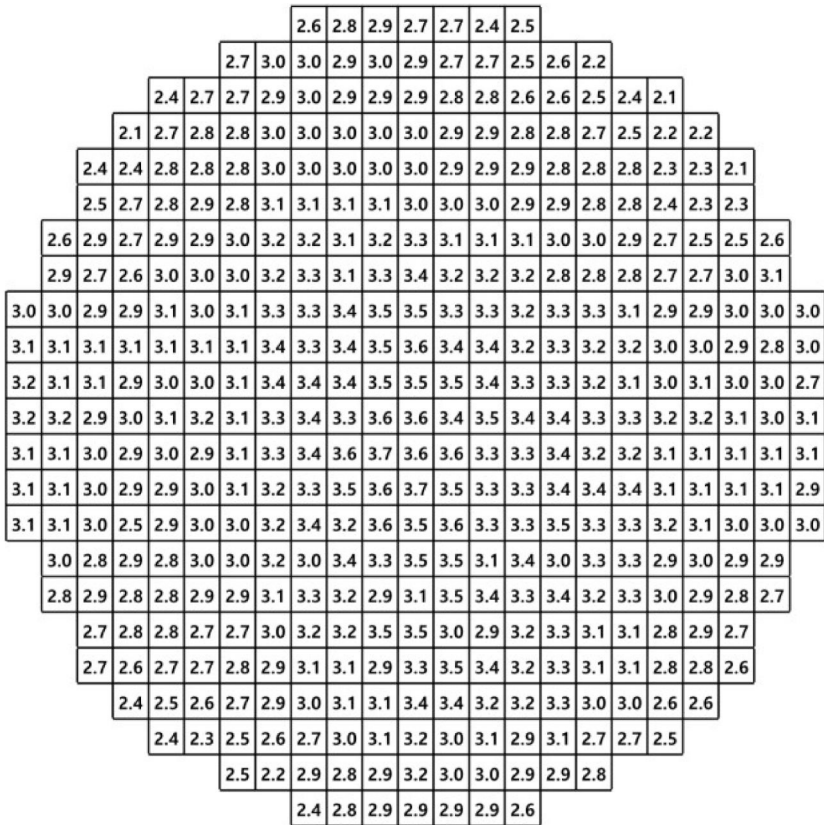**Figure 17.** Influence maps of one quadrant of the DM.

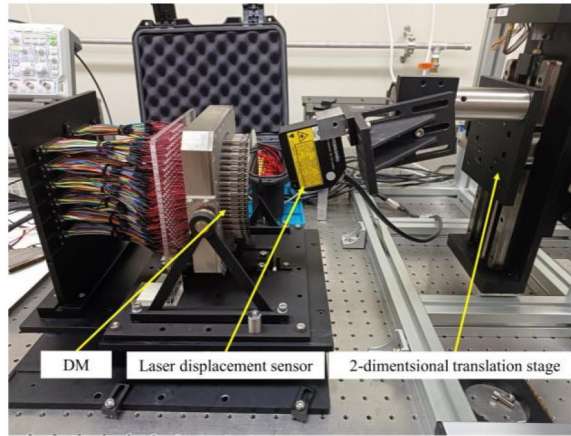**Figure 18.** Measurement results of the mirror surface strokes.

Figure 19. Measurement setup to measure the dynamic response of mirror surface stroke.
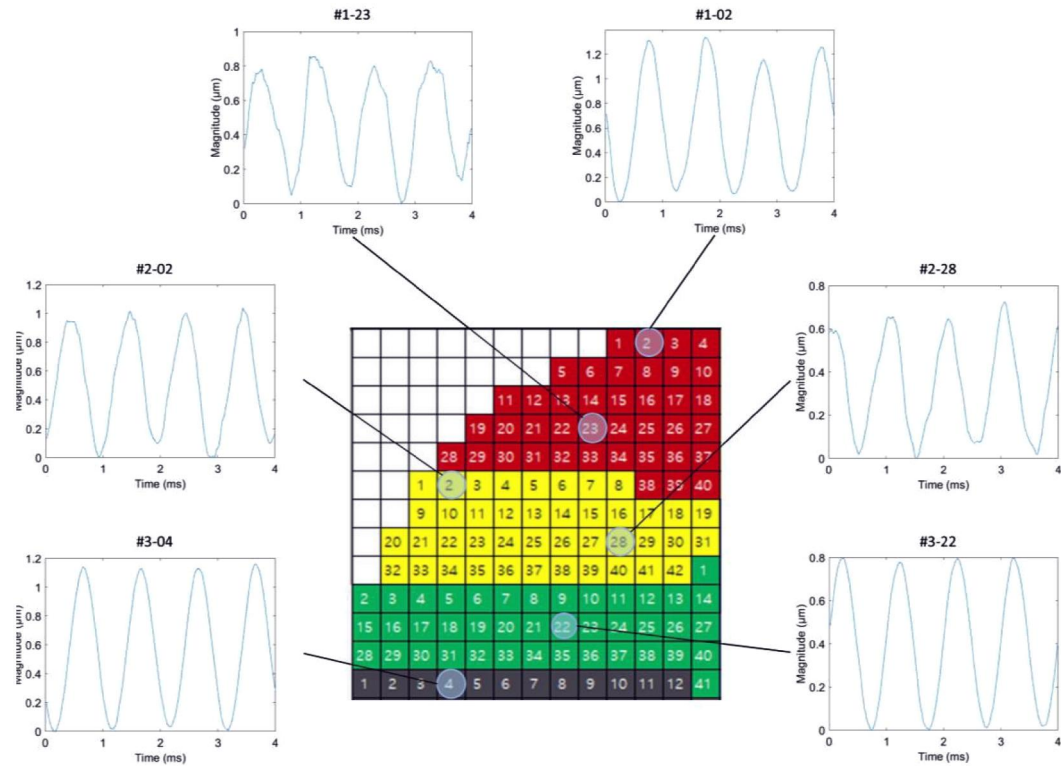

Figure 20. Measurement result of the dynamic responses of the SiC DM.

Figure 20 shows the measured dynamic response in one quadrant of the DM. The mirror surface stroke resulting from the operation of a single actuator properly follows the 1 kHz input frequency, indicating that the DM meets the design target: the dynamic response of the mirror surface from a single actuator operation ≥ 1 kHz.

5.3. Test of the coupling ratio

The coupling ratio is defined where a continuous mirror faceplate is applied. This value affects the ability of the DM to compensate for wavefront errors, and it is affected by factors such as the

thickness and stiffness of the mirror faceplate, the spacing of actuators, the attachment conditions between the mirror faceplate and the actuators, and so on. Therefore, the design coupling ratio of a DM varies based on its target level of wavefront error correction, as well as its material and structural specifications. The coupling ratio of a DM refers to the ratio of the mirror stroke at a neighboring deactivated actuator position to that of an activated actuator position. This is expressed as Equation (1).

$$\text{Coupling ratio} = (\text{Mirror stroke at the neighboring deactivated actuator}/ \text{Mirror stroke at the activated actuator}) \times 100\% \tag{1}$$

In Figure 17, the box outlined by the dotted blue line represents the position at which the minimum coupling ratio occurs, while the box outlined by the solid blue line indicates the position of the maximum coupling ratio. By comparing the mirror surface strokes at two adjacent actuator positions in the DM, the measurements show that the minimum coupling ratio is 28%, with a maximum value of 52%. It was observed that the coupling ratio decreases from the center toward the boundary. As a result, it is confirmed that the coupling ratio is within the designed range: 15–70%.

6. Conclusions

In this paper, a new line module type of DM with a SiC mirror faceplate is developed, and the performance of the DM is tested. The DM is designed to be suitable for an AO system used under Korean atmospheric conditions. Owing to the introduction of the line module concept, the assembly process of the base plate and the actuators becomes simpler and more stable. It minimizes the risk of actuator breakage during assembly and allows for easy exchange of a line module if defective actuators are found. Through alignment tolerance checks for each line module and across the line modules, the possibility of lateral and height misalignments of the actuators is minimized. Simulations of the line module type DM under gravity and temperature variations are performed, and the results show that the deformations of the mirror faceplate are sufficiently low to be easily compensated by small strokes of actuators. To prevent mirror distortion when the DM is mounted in the horizontal direction, bipod stands and a bottom flexure are applied. Assessments show that the bipod stands are reliable against small position errors of the fixed points in terms of the mirror surface distortion. To integrate the components, a delicate assembly process is utilized in order to secure the surface quality of the mirror faceplate and the ideal adhesive thickness. As a result of the assembly, all components are firmly glued together without any broken parts.

For validation of the developed SiC DM, performance tests are conducted. First, the mirror surface shape is measured with a Fizeau interferometer while electric power is supplied to each actuator. The stroke at each actuator position exceeds $2\,\mu\text{m}$, and it is shown that the shape of the surface deformation during the activation of each actuator is correct. Next, the dynamic response of the mirror surface stroke is measured with a laser displacement sensor. For successful wavefront error compensation, a 1 kHz response is required, and the measured result meets this requirement. Lastly, the coupling ratios are evaluated in the horizontal and diagonal directions. By comparing the mirror surface strokes of the activated actuator position and the neighboring deactivated actuator position, the coupling ratio is calculated, with the results showing that the coupling ratios are within the designed range: 15–70%.

In this study, the proper design, preparation, fabrication, and assembly of the components of a SiC DM, as well as the performance testing of the DM, are performed. In future work, wavefront error correction will be carried out using a complete AO system equipped with the developed DM. Additionally, for higher-frequency HPL applications requiring longer ranges and higher altitudes, an active cooling system, high-reflectivity mirror coatings, the examination of the

applicability of faster actuators with a thin SiC mirror faceplate, and other considerations will be necessary. Since the SiC DM is applicable to AO systems in various fields, we expect that this research will provide meaningful fundamental information pertaining to the future development of DMs.

Disclosure statement

The authors declare no conflicts of interest.

Funding

ORCID

Pilseong Kang (iD) http://orcid.org/0000-0002-2618-9249
Jaehyun Lee (iD) http://orcid.org/0000-0001-5456-124X
Hyug-Gyo Rhee (iD) http://orcid.org/0000-0003-3614-5909

References

[1]   Arnon, S.; Kopeika, N. S. Adaptive optical transmitter and receiver for space communication through thin clouds. *Appl. Opt.* **1997**, *36*, 1987–1993. DOI: 10.1364/ao.36.001987.

[2]   Albert, O.; Sherman, L.; Mourou, G.; Norris, T. B.; Vdovin, G. Smart microscope: An adaptive optics learning system for aberration correction in multiphoton confocal microscopy. *Opt. Lett.* **2000**, *25*, 52–54. DOI: 10.1364/ol.25.000052.

[3]   Sherman, L.; Ye, J. Y.; Albert, O.; Norris, T. B. Adaptive correction of depth-induced aberrations in multiphoton scanning microscopy using a deformable mirror. *J. Microsc.* **2002**, *206*, 65–71. DOI: 10.1046/j.1365-2818.2002.01004.x.

[4]   Fernandez, E. J.; Vabre, L.; Hermann, B.; Unterhuber, A.; Povazay, B.; Drexler, W. Adaptive optics with a magnetic deformable mirror: Applications in the human eye. *Opt. Express.* **2006**, *14*, 8900–8917. DOI: 10.1364/oe.14.008900.

[5]   Madec, P.-Y. 2012 Overview of deformable mirror technologies for adaptive optics and astronomy. In *Proceeding of the SPIE 8447*. DOI: 10.1117/12.924892.

[6]   Carroll, J.; Kay, D. B.; Scoles, D.; Dubra, A.; Lombardo, M. Adaptive optics retinal imaging – Clinical opportunities and challenges. *Curr. Eye Res.* **2013**, *38*, 709–721. DOI: 10.3109/02713683.2013.784792.

[7]   Booth, M.; Andrade, D.; Burke, D.; Patton, B.; Zurauskas, M. Aberrations and adaptive optics in super-resolution microscopy. *Microscopy (Oxf).* **2015**, *64*, 251–261. DOI: 10.1093/jmicro/dfv033.

[8]   Rigaut, F.; Neichel, B. Multiconjugate adaptive optics for astronomy. *Annu. Rev. Astron. Astrophys.* **2018**, *56*, 277–314. DOI: 10.1146/annurev-astro-091916-055320.

[9]   Roberts, L. C.; Meeker, S. R.; Tesch, J.; Shelton, J. C.; Roberts, J. E.; Fregoso, S. F.; Troung, T.; Peng, M.; Matthews, K.; Herzog, H.; Rodriguez, J. Performance of the adaptive optics system for laser communications relay demonstration's ground station 1. *Appl. Opt.* **2023**, *62*, G26–G36. DOI: 10.1364/AO.486752.

[10]   Freeman, R. H.; Garcia, H. R. High-speed deformable mirror system. *Appl. Opt.* **1982**, *21*, 589–595. DOI: 10.1364/AO.21.000589.

[11]   Kudryashov, V.; Samarkin, V. V. Control of high power CO_2 laser beam by adaptive optical elements. *Opt. Commun.* **1995**, *118*, 317–322. DOI: 10.1016/0030-4018(95)00218-W.

[12]   Kudryashov, V.; Samarkin, V. V.; Rukosuev, A. L.; Alexandrov, A. "High-power lasers and adaptive optics," laser resonators and beam control VII. *SPIE* **2005**, *5333*, 45–52.

[13]   Vinevich, S.; Evdokimovich, L. N.; Smirnov, S. N.; Safronov, A. G. Controlling the output radiation power of Co2 lasers by means of deformable mirrors. *J. Opt. Technol.* **2004**, *71*, 65–70. DOI: 10.1364/JOT.71.000065.

[14]   Rabczuk, G.; Sawczak, M. Study on the possibilities of controlling the laser output beam properties by an intracavity deformable mirror. *Opto-Electronics Rev.* **2006**, *14*, 136–142. DOI: 10.2478/s11772-006-0018-9.

[15] Sprangle, P.; Hafizi, B.; Ting, A.; Fischer, R. High-power lasers for directed-energy applications. *Appl. Opt.* **2015**, *54*, F201–F209. DOI: 10.1364/AO.54.00F201.
[16] Ahn, K.; Rhee, H. G.; Yang, H. S.; Kihm, H. Silicon carbide deformable mirror with 37 actuators for adaptive optics. *J. Korean Phys. Soc.* **2015**, *67*, 1882–1888. DOI: 10.3938/jkps.67.1882.
[17] Ahn, K.; Rhee, H. G.; Yang, H. S.; Kihm, H. CVD SiC deformable mirror with monolithic cooling channels. *Opt. Express.* **2018**, *26*, 9724–9739. DOI: 10.1364/OE.26.009724.
[18] Han, K.; Cui, W.; Yang, Y.; Xi, F.; Li, X.; Du, S. Evaluating the potential of laser beam quality improvement by adaptive optics system. *Int. J. Opt.* **2019**, *2019*, 1–6. DOI: 10.1155/2019/1970406.
[19] Zhang, Y.; Lv, X.; Long, G.; Zhou, H.; Cheng, L. Study on the cooling method of deformable mirror under laser irradiation." In *10th International Symposium on Advanced Optical Manufacturing and Testing Technologies: Large Mirror and Telescopes.* 2021; pp. 160–168. DOI: 10.1117/12.2603866.
[20] Kang, P.; Huh, J.; Lee, K.; Park, S.; Rhee, H. G. Design of a discrete flexure for a SiC deformable mirror with PMN stacked-actuators. *Opt. Express.* **2021**, *29*, 31778–31795. DOI: 10.1364/OE.436362.
[21] Bae, J. Y.; Hur, H.; Kim, I. J.; Lee, K.-S.; Kihm, H.; Rhee, H.-G.; Yang, H.-S.; Kim, H.-S.; Hyun, S. Experimental and numerical investigations on cooling performance of chemical-vapor-deposited SiC deformable mirror for adaptive optics system in high-power laser radiation environments. *Appl. Therm. Eng.* **2022**, *203*, 117950. DOI: 10.1016/j.applthermaleng.2021.117950.
[22] Rukosuev, L.; Nikitin, A. N.; Galaktionov, I. V.; Sheldakova, Y. V.; Kudryashov, A. V., M.A. Sadovsii Institute of Geoshpere Dynamics RAS. Real-time adaptive optics for high-power laser beam correction in the strong turbulence. *Comput. Opt.* **2024**, *48*, 511–518. DOI: 10.18287/2412-6179-CO-1352.
[23] Holmes, R. B. Adaptive optics for directed energy: Fundamentals and methodology. *AIAA J.* **2022**, *60*, 5633–5644. DOI: 10.2514/1.J061766.
[24] Babcock, H. W. The possibility of compensating astronomical seeing. *PASP.* **1953**, *65*, 229–236. DOI: 10.1086/126606.
[25] Ealey, M. A.; Wellman, J. A. Cooled ISOFLOW laser mirrors. *High Heat Flux Eng.* **1993**, *1739*, 374–382.
[26] Jana, D. C.; Saha, B. P. Silicon carbide-based lightweight mirror blanks for space optics applications. In *Handbook of Advanced Ceramics and Composites: Defense, Security, Aerospace and Energy Applications*; Springer: Cham, 2020; pp. 1135–1163.
[27] 3M^{TM}, Schoch-Weld^{TM} Epoxy Adhesive 2216 B/A Technical Data. 2018.